Experimental Mechanics (2017) 57:1395–1409
DOI 10.1007/s11340-017-0303-1

# Distortion Correction Protocol for Digital Image Correlation after Scanning Electron Microscopy: Emphasis on Long Duration and Ex-Situ Experiments

A.W. Mello[1] · T.A. Book[1] · A. Nicolas[1] · S.E. Otto[1] · C.J. Gilpin[2] · M.D. Sangid[1]

Received: 21 September 2016 / Accepted: 19 June 2017 / Published online: 13 July 2017


**Abstract** Recently, scanning electron microscopy (SEM) has been used for digital image correlation (DIC), as micrographs can be acquired with high magnification, providing improved resolution to quantify strain heterogeneities. However, it has been shown by researchers that SEM images can be problematic due to inherent electromagnetic distortions that are not present in optical images. Drift, spatial distortions, and magnification uncertainties are the main issues that can seriously affect the accuracy of localized strain measurements. The present work focuses on long duration experiments, for which images are taken days or weeks apart. We have proposed a systematic procedure to reduce drift, correct spatial distortion, and account for magnification variations between pairs of acquired images. Additionally, SEM parameters are discussed and chosen to increase the signal-to-noise ratio and improve the accuracy of the DIC measurements. The spatial distortion correction increases the repeatability of the correlated values and the precision of the measurements. The implementation for this type of correction is done by applying the measured distortion gradient of a certified grid onto the DIC strain field. The magnification adjustment increases the reliability of the strain maps, ensuring the measurements are in agreement with the actual strain induced during the experiment. We have presented a systematic protocol for ex-situ DIC experiments within the SEM and some basic cross-check procedures that can be performed to evaluate the reliability of the reference grid and the precision of the final strain map.

**Keywords** Microstructure · Digital image correlation · Scanning electron microscopy · Electron backscatter diffraction · Strain localization · Image distortion

✉ M. D. Sangid
msangid@purdue.edu

[1] School of Aeronautics and Astronautics, Purdue University, 701 W. Stadium Ave, West Lafayette, IN 47907, USA

[2] Life Science Microscopy Facility, Purdue University, 170 S. University St, West Lafayette, IN 47907, USA

## Introduction

Digital Image Correlation (DIC) has become a very important tool within the mechanics community to resolve strain heterogeneities. Additionally, DIC has been coupled with characterization techniques to identify microstructural features, which has enabled the ability to resolve localized grain and sub-grain level strains in polycrystalline materials (depending on the grain size of the material compared to the speckle size and distribution). Since the DIC technique is independent of length scale, the resulting resolution of strain is only limited by capturing fine details within the correlated image. To properly accomplish this task, speckle sizes using SiC particles on the order of 1 μm can easily be resolved and correlated by means of optical images [1, 2]. Yet, any speckle smaller than 1 μm will be very difficult to resolve and correlate from optical images. DIC associated with scanning electron microscopy (SEM) imaging has improved the capability of strain localization studies, by increasing the magnification and the resolution within the grains [3–7].

Sutton et al. [8–10] have called attention to and proposed corrections for SEM inherent distortions that could lead to inaccurate displacement field measurements. They classified the distortions as spatial and time varying drift, and postulated that spatial distortion is more pronounced for low magnifications, while drift distortion dominates at high magnifications [8]. The methodology proposed by Sutton et al. [8] required

the acquisition of several images of a speckled surface at the same and different positions. Variation in time will account for drift, and variation in position will be considered spatial distortion. For the drift correction, they correlated consecutive images in pairs to obtain drift disparity maps, defining a time-based drift function at each disparity point. The correlation of translated images accounted for spatial distortion, and to obtain the disparity map in this case, they compared the DIC displacements with the known commanded stage position. The vulnerability of this procedure is that it considers the positions (X, Y) of the stage as deterministic. However, even ultra-high resolution SEMs currently available will have a stage repeatability on order of 0.5 μm [11]. In the same work, Sutton et al. recognized this issue and others, such as the translation stage control systems are generally prone to backlash and/or overshoot and difficulty maintaining the orientation of the stage (X and Y movements are not decoupled). Finally, Sutton et al. [8] stated that accurate grid targets are the natural choice to quantify non-parametric spatial distortions. However, at that time, it was difficult to acquire an accurate grid target to resolve SEM resolution at the micro- or nano-scale. With the evolution of lithography and nanotechnology, we will reexamine this topic, as discussed in the sections to follow, and provide an alternate method for SEM-DIC spatial correction that is more suitable for ex-situ experiments.

SEM image distortions are a major concern, especially with increasing resolution of the acquired DIC strain fields. For instance, Kammers and Daly [12] used a self-assembled gold nanoparticle surface patterning technique to enable nanometer resolution. They could achieve 4 nm/pixel resolution from SEM images. Working at that resolution, Kammers and Daly [13] have presented a complimentary methodology and validation for corrections of SEM image distortions. In this work, they implemented the procedures proposed by Sutton [8–10], and showed that for in-situ experiments, the material stress relaxation has to be accounted for concurrently when correcting for drift. The displacements caused by stress relaxation are inherent to the material and they should not be removed by imposing a drift distortion correction. This paper focuses on ex-situ techniques that are not susceptible to material stress relaxation, and through proper procedure the drift is minimized. In addition to all good practices for distortion correction, Stinville et al. [14] proposed a methodology to reduce noise during SEM image acquisition, and DIC parameters adjustment to minimize the distortions' effect on the mapped strain field. With this approach, noise will be low, drift will be minimized and spatial distortion will account for feasible SEM-DIC correction.

When focusing on ex-situ experiments, the calibration and repeatability of the reported magnification values need to be consistent when performed over various SEM sessions. As pointed by Dai et al. [15], the classical SEM magnification calibration protocol is not sufficient to provide high accuracy magnification settings; and they demonstrated a magnification could be calibrated using a certified grid and correction via Fourier transform. Additionally, Tortonese et al. [16] discussed the proper method and limitations for using a certified grid for calibration inside a SEM. Despite all efforts for magnification calibration, we show that even with the same magnification and field of view, there is always some slight variation in the actual scale of SEM images acquired during disparate SEM sessions. The importance of this matter comes from the fact that we have to deal with the outstanding issue that small deviations in the magnification will manifest into large discrepancies in the reported strains via DIC measurements.

In the present work, we discuss the parameters that affect drift and spatial distortions of a SEM image. We have evaluated the current, spot size, aperture size, and described other procedures to obtain optimal acquisition conditions for DIC. The objective of showing the optimization parameters for our specific case is to call attention to the fact that noise and drift can be minimized. A certified grid is used as reference for creating a spatial correction displacement field, which offers a full field method for spatial correction compared to a series of individual images proposed by Sutton et al. [10]. We have evaluated the grid in terms of resolution and reliability. The emphasis of the present distortion correction procedure is for long duration tests, including fatigue or creep, where ex-situ methods are necessary. For the ex-situ method, the certified grid that is placed beside the tested sample is also used as a calibration image, which is acquired after each session to ensure the magnification readings are consistent and repeatable over different SEM sessions (without the need to re-calibrate the SEM during each session). We have also derived a distortion gradient field from the grid corrections that can be applied directly to the strain field, thus allowing the full capability and filters of a commercial software to generate the final strain maps. As a main contribution of this paper, we present a systematic protocol that can be easily reproduced and applied in future high-resolution DIC studies.

## Methodology

In this section, a systematic protocol is presented for obtaining high spatial resolution strain fields by DIC within an SEM, by means of long duration, ex-situ testing. Specifically, the SEM parameters are presented to reduce noise and minimize drift, followed by a detailed methodology to correct for spatial distortions during the measurement technique, and finally the uncertainty quantification of the reported magnification from the SEM. In this study, the materials examined are a Ni-based superalloy and a Ti-6Al-4V alloy, speckled with self assembled nanoparticles according to the methodology presented in

[12]. All imaging was performed at the Purdue Life Science Microscopy Facility. Two microscopes were used to check the results, the FEI NOVA nanoSEM and FEI Quanta 3D FEG field emission scanning electron microscopes (FEI Company, Hillsboro Oregon), both using an ET (Everhart-Thornley) detector operated at 5 kV accelerating voltage.

## Drift Minimization and Appropriate Parameters for Noise Reduction

As a sample is scanned by a focused beam of electrons, the image can be affected by charging effects. As a consequence, an image acquisition is subjected to a time varying distortion of pixels in consecutive captured images, which is known as drift. Charge induced drift may exhibit random orientation and varying speed [13]. The direction of this movement is subsequently difficult, if not impossible, to predict. Additionally, the translational uncertainty caused by drift may be exacerbated by imprecision in the positioning stage holding the specimen within the SEM. Any moving stage has a relaxation period that may cause movements similar to beam drift. Even high resolution motorized stages can move up to 20 nm per minute for the first 15 min after last commanded movement [17]. The best way found to minimize these drifting effects is to prepare the sample and deal with the setup parameters accordingly.

One way to minimize drift is to properly ground the specimen to make sure the current in the specimen is completely drained of electrical charging. In our ex-situ experiments, the sample and the grid are fixed in the holder by carbon tape, and both ends of the specimens are connected to the holder with copper tape. At both edges, the copper tape is folded, forming a ~ 1 mm point of contact with the specimen and holder without the use of glue. This technique provides excellent grounding for the specimen. To guarantee the satisfactory grounding, an ohmmeter is used to measure the resistance between specimen/grid and stage. Figure 1 shows a speckled specimen and a grid on the holder with improved connectivity between sample and stage.

To choose the best parameters for DIC, pairs of images were captured and subjected to slight rigid body movement with exactly the same acquisition settings. Each pair of images is then correlated and the standard deviation of axial strain is computed for choosing the optimum subset size [1]. The SEM acquisition parameters are then systematically changed following an optimization procedure based on minimizing the standard deviation of strain that provides a pair of images (with little noise and adjacent to each other) with an average zero-strain. For the DIC, we aim for the minimum possible subset size, in order to obtain high spatial resolution of the reported strain fields from DIC. The larger the subset size, the larger the capability to capture the extreme high and low strain magnitudes, but compromising spatial resolution and localization measurements.

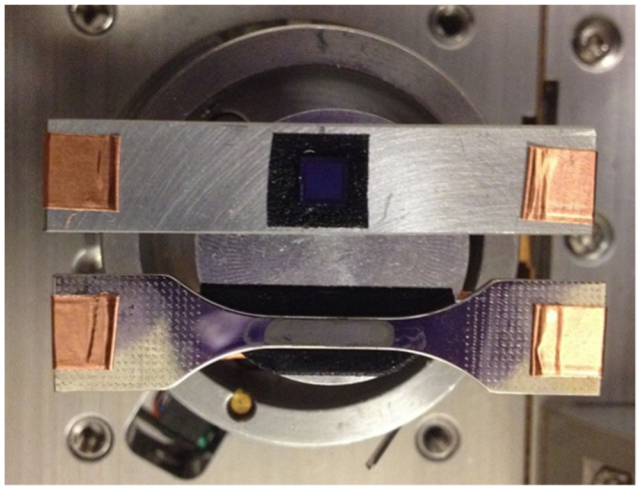

**Fig. 1** Specimen and grid on the holder with improved grounding setup

Considering the SEM imaging process [9], a lower accelerating voltage is important to avoid charging and to get better information and contrast of the surface speckles. High accelerating voltage will provide more information of the substrate under the surface portion, which may harm the correlation. For all our experiments, we have used a 5 kV accelerating voltage. For both FEI NOVA nanoSEM and FEI Quanta 3D FEG field emission scanning electron microscopes, this acceleration voltage provided a good contrast between speckles and substrate.

Probe current is determined by the size of the probe, which is directly related with the number and size of apertures and the control current of the condenser lens. We have investigated the effect of the probe current on the signal-to-noise ratio of acquired images. This is a very important guide for minimizing noise and distortions inherent to the SEM for the purpose of measuring strain fields via DIC. To do that, we systematically changed the current while taking pairs of images, for a Ti-6Al-4V specimen. Figure 2 shows the improvement of DIC accuracy with probe current and subset size. For large subset sizes, lower current is suitable, however, as previously discussed, this result will compromise the DIC resolution. Figure 3 shows the standard deviation of image pairs as a function of probe current, for a normalized 1 μm subset size. These results are in agreement with an extensive study by Stinville et al. [18], relating accuracy with subset size. The dependency with probe current, a consequence of changing the electron probe diameter, can be explained by the fact that for a higher probe current, more secondary electrons and backscattered electrons are emitted, increasing the probe size and the signal intensity. Therefore, probe current is a trade-off between noise reduction and resolution. As can be seen in Fig. 3, the improvement in accuracy for a defined subset size is saturated for values above 53 pA of probe current. The

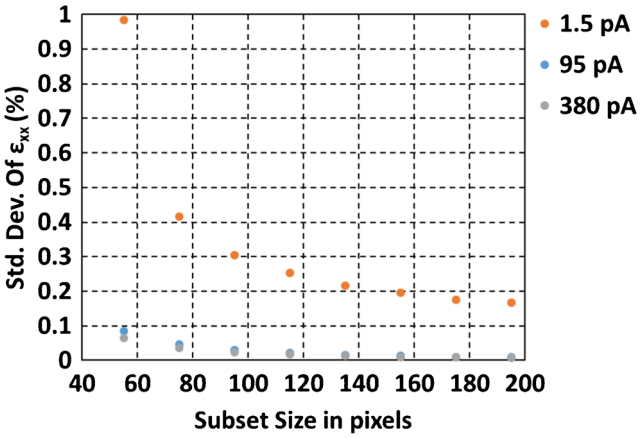


**Fig. 2** Subset size versus standard deviation of $\varepsilon_{xx}$ for 1.5 pA, 95 pA and 380 pA

purpose of this study is to describe a methodology that will work with all SEM systems, it is not intended to give an absolute value of current.

Another crosscheck performed for improving the signal-to-noise ratio and repeatability of features was the influence of spot and aperture size. Figure 4 depicts our measurement of the accuracy of the DIC characterization based on standard deviation of $\varepsilon_{xx}$ as a function of spot and aperture size. As can be seen, the increase in resolution of pixel acquisition based on smaller spot size must go with the increase of aperture size to maintain satisfactory accuracy.

Finally, Fig. 5 shows the influence of pixel acquisition dwell time and post-processing integration filter in the reference DIC standard deviation for a subset size of 1 μm, similar to the procedure described by Sutton et al. [8, 9]. The acquisition dwell time is the amount of time while the electron beam is at a single pixel position. For low dwell time, normally it is necessary to employ a post-processing filter to average acquisition passes. Image processing can be used for the improvement of image visual display and analysis, and integration techniques can be applied to a sequence of images to highlight differences between pixel values. Integration will

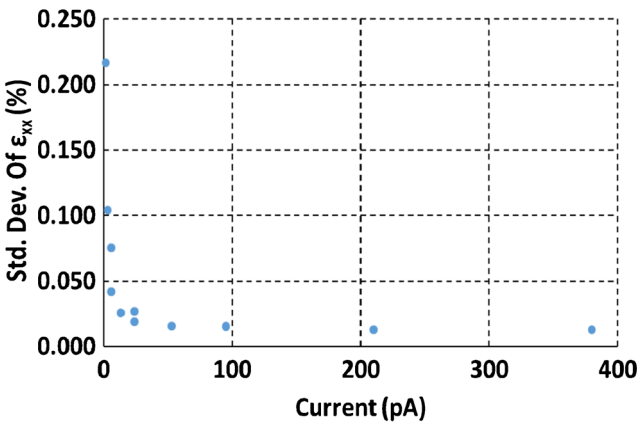


**Fig. 3** DIC accuracy from pairs of reference images as a function of probe current for a subset size of 1 μm

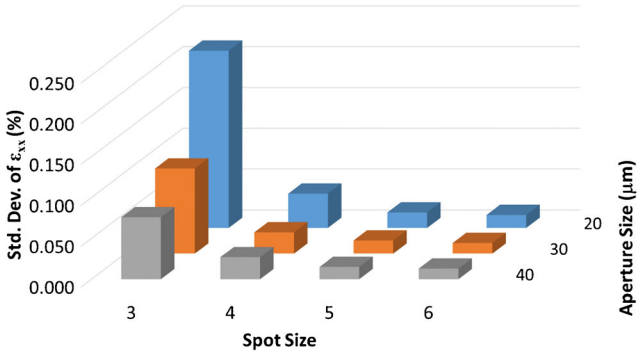


**Fig. 4** Effects of aperture size and spot size on $\varepsilon_{xx}$ standard deviation for a subset size of 1 μm and probe current of 53 pA

work better if drift is very low, otherwise any type of post-processing may compromise resolution. For any type of filter, it is very important to assess the accuracy of the data with the repeatability of the results. In our experiments, the best condition determined for DIC is to increase pixel acquisition dwell time with single integration.

After all these experimental checks, we can say that the ideal condition for DIC is not to optimize any single parameter but to find the lowest current (combination of accelerating voltage, spot size, dwell time, and aperture) that minimizes the standard deviation of strain between image pairs. For the case of the set-up used in this study (Fig. 3), the ideal current is 53 pA for both Ni and Ti specimens, which represents sufficient signal-to-noise that no integration or averaging of images are required. Any integration or average at this point may be detrimental and result in an increase in the standard deviation of the strain among the image pairs, thereby increasing overall experimental error. The ideal current is unique to a particular test and speckle material and must be experimentally re-determined if either the material or speckle is changed. In this paper, two different materials and speckles are evaluated for distortion correction. For these cases, the SEM parameters for (i) the Ni-base superalloy sample are: magnification 3,500×, spot size 3, and work distance of 5 mm, and (ii) for the Ti-6Al-4V sample are: magnification 8,000×, spot size 5, and working distance 10 mm. As noted, a methodology for

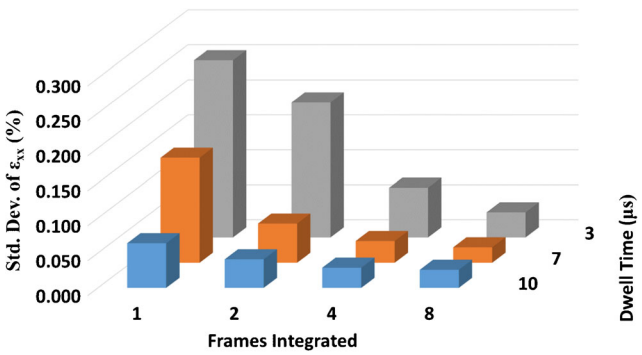


**Fig. 5** Influence of dwell time and real time integration on DIC accuracy for a subset size of 1 μm and probe current of 53 pA

determining the specific SEM parameters are not intended to be transferable across all SEM systems, but rather this protocol needs to be followed to identify the appropriate combination of parameters for each SEM system (as a single parameter on its own is not sufficient to minimize DIC error).

## Spatial Distortion Correction

For the application of this methodology, it is very important to keep all parameters precisely the same, from the calibration phase until the last DIC acquired image. For the results presented in this work, we used the signal-to-noise acquisition optimization described in "Drift Minimization and Appropriate Parameters for Noise Reduction" section.

### *Procedure overview*

The methodology consists of using a calibration image with known, uniform, and well defined feature pattern to determine the distortion field [19]. In sequence, this distortion field is used to correct DIC computed strains. Considering that the underlying SEM distortion mechanisms are from multiple sources, the calibration image must be acquired precisely in the same way as the desired images in terms of pixel resolution, magnification, accelerating voltage, spot size, working distance, and acquisition parameters, such as dwell time, integration or averaging methods. Additionally, all subsequent images are acquired by replicating the brightness and contrast of the reference images, to minimize gray level and blur effect. Charbal et al. [20] have proposed image corrections when the gray level is accentuated, although this is beyond the scope of the current paper. Any available method must be used to reduce the random variation and noise in the images. As mentioned before, the proper grounding of the specimen is necessary to considerably reduce the drift during acquisition.

For the purpose of clarity in the methodology development, let us consider a simple image, which contains regularly spaced and perpendicular features, deformed as depicted in Fig. 6 (a). By identifying the average horizontal and vertical vectors among rows and columns of features, we will find the reference vectors $\boldsymbol{u}$ and $\boldsymbol{v}$ shown in Fig. 6(a). Using a designated point as reference, the vectors will be orthogonalized and redefined forming an orthonormal basis. All the features will be moved according to an updated position in the new coordinate system, as illustrated in Fig. 6(b).

The perpendicular vectors are used to construct the physically correct grid of features centered on the reference point. The displacements between each feature center, or grid targets, in the calibration image and the physically correct centers is determined. The displacement field is found by interpolating the displacements of mapped grid points. In the example of Fig. 6, the displacement field would be obtained by interpolation among all 25 known movements to bring points from condition (a) to condition (b), represented in Fig. 6. Finally, the displacements are used to generate a bi-cubic surface that can be visualized as a distortion field of the typical SEM. An advantage of using a well defined pattern, as opposed to translation of a random speckle pattern as described in [8, 9, 13] is to avoid the dependence of an accurate translational stage in the distortion correction protocol. The accuracy and resolution of the grid targets will be further discussed in "Grid Accuracy and Resolution" section.

### *Distortion field*

For the framework and results in this paper, a 3 × 3 mm (total size) high precision, individually certified Pelcotec™ G-1C Silicon Calibration Specimen was used, with 1 μm pitch, certified according to working standards traceable to the National Institute of Standards and Technology with uncertainty within 0.005 μm, which is more accurate than most positioning stages. The grid was placed on a specimen-like strip (i.e. same thickness) and attached to the holder as shown in Fig. 1. The grid lines are 150 nm wide. Despite the pattern repetition being 1 μm, that is, according to our recognition protocol, the minimum distance between identified features to generate the reference grid for distortion correction, just a few points are necessary to generate a distortion field by interpolating the chosen disparity points [8, 13]. In this paper, we have worked with 10 μm distance between mapped features. To generate the distortion field, a code was written to identify the features in the calibration grid. Figure 7 shows a grid with highlighted subset *tiles* to illustrate the mapping. In this code, the user can define the size of the *tile* that will be tracked to map the reference points. This *tile* is identified within a subset on the screen. The program recognizes the same *tile* at a certain distance from the first position and so on. The code searches for the same *tile* at a given distance and looks around for the best match. The best match is found by minimizing the pixel intensity differences inside the *tile*. Let us consider a subset tile with $n \times n$ pixels, as shown in Fig. 7. If $I_{Refi,j}$ is the normalized intensity of the pixel in positon $(i, j)$ in the reference subset, the matching subsets will be found by minimizing

$$\sum_{i=1}^{n}\sum_{j=1}^{n}\left(I_{k_{i,j}} - I_{\mathrm{Re}f_{i,j}}\right)^2 \quad (1)$$

where $I_{ki,j}$ is the pixel normalized intensity in position $(i, j)$ in the subset k. The center of the subset will be assigned as the reference point. The positions are defined with subpixel resolution, because (a) the subset tile can contain as many pixels as necessary for a stable and repeatable recognition of equidistant features and (b) each target is averaged and set at exactly the same distance to each other. This protocol works for any type of grid or feature orientation.

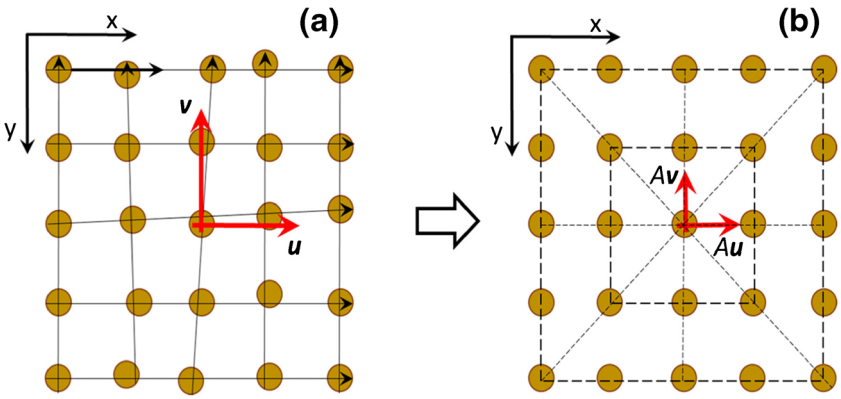


**Fig. 6** (a) Regularly spaced and orthogonal grid points shown distorted for representation purpose. (b) Orthogonal transformation from previously known spacing and perpendicularity of features

Figure 8 shows the same grid, where the program was set to recognize a grid reference point every 10 μm. In this case, the program could map 9 columns and 8 rows for a total of 72 reference points. After identifying the grid points, the code determines the basis vectors with the origin on a reference point. The first identified point is used as reference (top left). The choice of the origin does not affect the final result, since the distortion field gradient will be used for strain computation. It can be noticed from Fig. 8, that the grid displays some non-orthogonality, especially in the bottom right subset. This is a typical distortion found in SEM images [21], and it is present with the same intensity in all images acquired at the same magnification. With proper manufacturer calibration [21], this non-orthogonality can be reduced, but may reappear with time. The tolerance in orthogonality accuracy is on the order of 2% according to the standards of scanning electron microscopes [21]. The current procedure corrects this and all other spatial distortion in the DIC images.

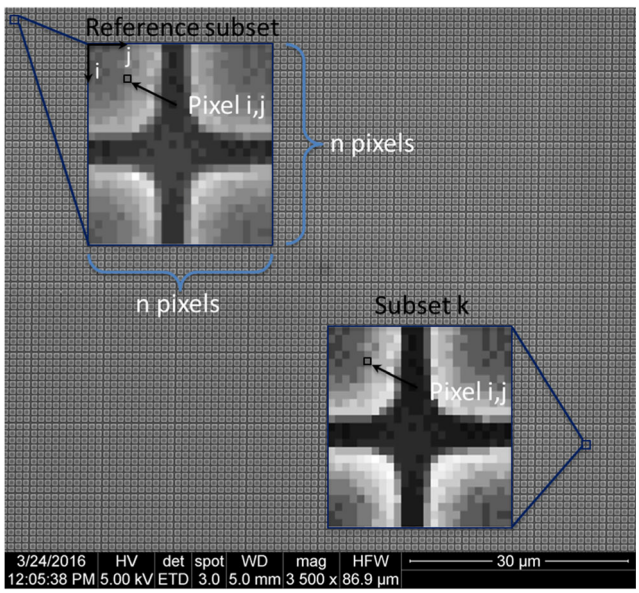


**Fig. 7** SEM Image of Pelcotec™ G-1C Silicon Calibration Specimen, at 3,500× magnification, with highlighted subset tiles for pattern repetition mapping

As can be seen in Fig. 8(a), the match point was set as the top left. It causes a maximum cumulative distortion to be measured at the bottom right of the grid (Fig. 8(b)). After the determined grid distortion points are mapped, the positons with their respective horizontal and vertical displacements are used to generate a bicubic distortion surface. Let's consider the discrete disparity points *f(x, y)* obtained from the grid mapping plotted in the x-y plane of the image, as seen in Fig. 9(a). Because *f* only exists in the mapped points, let's represent *f* in the coordinates $\xi$, $\eta$, where $\xi = 1, 2, 3, \ldots m$ and $\eta = 1, 2, 3, \ldots n$, and *m* and *n* are the total of grid mapped points (targets) on *x* and *y* directions, respectively. For each pair ($\xi$, $\eta$), we know the corresponding (*x, y*) coordinate.

At each point ($\xi$, $\eta$), *f* is known from the grid mapping, and its derivatives can be estimated by:

$$f_x(\xi,\eta) = \frac{f(\xi+1,\eta) - f(\xi-1,\eta)}{2\Delta x} \tag{2a}$$

$$f_y(\xi,\eta) = \frac{f(\xi,\eta+1) - f(\xi,\eta-1)}{2\Delta y} \tag{2b}$$

$$f_{xy}(\xi,\eta) = \frac{f_x(\xi,\eta+1) - f_x(\xi,\eta-1)}{2\Delta y} \tag{2c}$$

A bicubic surface covering the area $A_k$, as shown in Fig. 9(b), can be interpolated using the above known values of the four corners, and can be written as:

$$p(x,y) = \sum_{i=0}^{3}\sum_{j=0}^{3} a_{ij} x^i y^j \tag{3}$$

By performing a proper change of coordinates (ξ', η'), as shown in Fig. 10, the function values *f* and the derivatives *fx, fy* and *fxy* are known at the four corners (0, 0), (1, 0), (0, 1), and (1, 1) of the unit square.

The interpolation is solved by determining the 16 coefficients $a_{ij}$, matching $p(x, y)$ with the four function values, eight equations for the derivatives in *x* and *y* directions and four cross derivatives *xy*, obtained in the four corner points of the

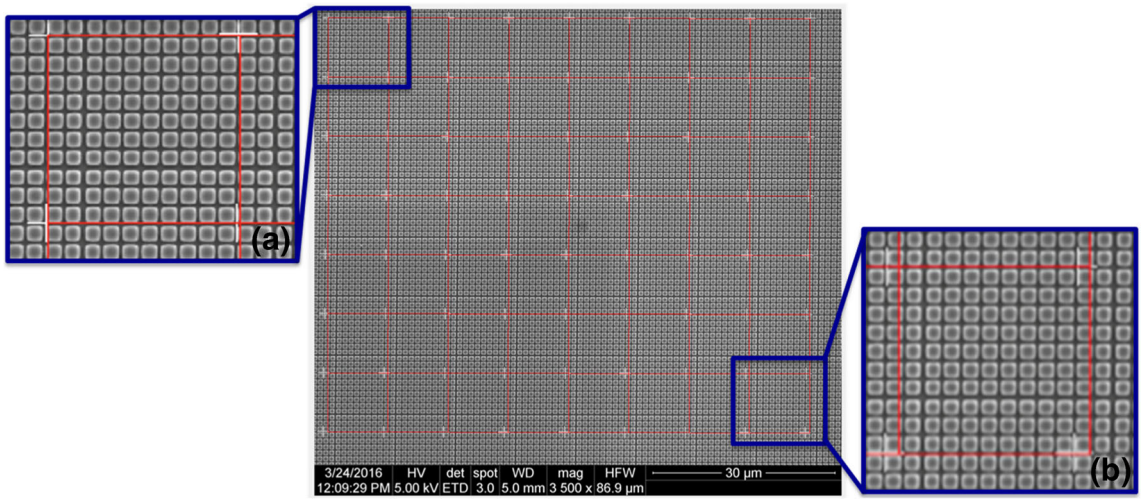


**Fig. 8** Spatial distortion mapped with SEM Image of Pelcotec™ G-1C Silicon Calibration Specimen, at 3,500× magnification

patch. In the new coordinate system (0-1) with proper manipulation, the coefficients $a_{ij}$ can be determined by:

$$\begin{bmatrix} a_{00} & a_{01} & a_{02} & a_{03} \\ a_{10} & a_{11} & a_{12} & a_{13} \\ a_{20} & a_{21} & a_{22} & a_{23} \\ a_{30} & a_{31} & a_{32} & a_{33} \end{bmatrix} = \begin{bmatrix} 1 & 0 & 0 & 0 \\ 0 & 0 & 1 & 0 \\ -3 & 3 & -2 & -1 \\ 2 & -2 & 1 & 1 \end{bmatrix} \tag{4}$$

$$\begin{bmatrix} f(0,0) & f(0,1) & f_y(0,0) & f_y(0,1) \\ f(1,0) & f(1,1) & f_y(1,0) & f_y(1,1) \\ f_x(0,0) & f_x(0,1) & f_{xy}(0,0) & f_{xy}(0,1) \\ f_x(1,0) & f_x(1,1) & f_{xy}(1,0) & f_{xy}(1,1) \end{bmatrix} \begin{bmatrix} 1 & 0 & -3 & 2 \\ 0 & 0 & 3 & -2 \\ 0 & 1 & -2 & 1 \\ 0 & 0 & -1 & 1 \end{bmatrix}$$

This procedure yields a surface $p(x, y)$ of (equation (3)) on the unit square [0,1] x [0,1] delimited for four points, which is continuous with continuous derivatives. The entire surface is covered by stitching together the bicubic surfaces, ensuring that the derivatives match on the boundaries. The derivatives are obtained from the following identities:

$$p_x(x,y) = \sum_{i=1}^{3}\sum_{j=0}^{3} a_{ij} i x^{i-1} y^{j} \tag{5a}$$

$$p_y(x,y) = \sum_{i=0}^{3}\sum_{j=1}^{3} a_{ij} x^{i} j y^{j-1} \tag{5b}$$

$$p_{xy}(x,y) = \sum_{i=1}^{3}\sum_{j=1}^{3} a_{ij} i x^{i-1} j y^{j-1} \tag{5c}$$

A preliminary verification can be done by applying the distortion correction directly to the grid image, interpolating the pixels. The newly corrected grid can be loaded in the distortion code and new displacement field should be a flat surface, exhibiting near zero gradient. This procedure can be used for verification purposes only to ensure the spatial correction is calculated correctly. The cross check verification on the grid has a similar purpose as Sutton et al.'s [8] simulation of the correlation between two reference images, in order to quantify the precision of the correction function fit for the strain maps. In our case, the image correction should not be applied to the raw deformed image prior to correlation, as it is not possible to move a fraction of a pixel. The disparity field has to be used to obtain the distortion gradient function that will be used for strain distortion correction as shown in sequence.

The gradient of the bicubic surface is determined using (equation (5a) and (5b)) mapping the image pixel by pixel. From the distortion map, we can define $p_u$ and $p_v$ as orthogonal distortions in the x and y directions, respectively. In this case, we solve the cubic interpolation in (equation (3)) for $p_u$ and $p_v$ independently. The gradient can then be composed with the results from a commercial software strain map to obtain the distortion-free Lagrangian strain fields, as proposed in [13]. In the present work, the following correction for the strain field is employed. Without loss of generality, consider two subsets being stretched in distorted and undistorted image

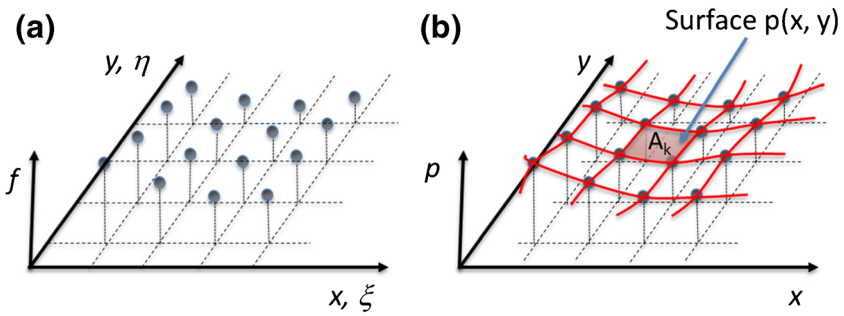


**Fig. 9** (a) Discrete distortion points from grid mapping, and (b) surface fit for the mapped points covering all the region

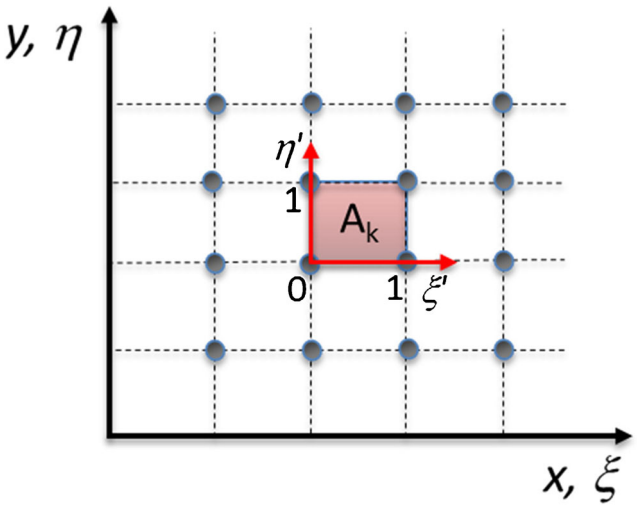


**Fig. 10** Change of coordinates for each patch, forming a unit square

pairs, as shown in Fig. 11, where the displacement geometric solution based on a predefined subset size is depicted as first order elements. It is important to notice that the commercial software uses the strained and unstrained images in the distorted system, which are the original acquired images, and the strains are computed based on a subset size.

The corrected stain field is then computed as a composition of the distorted strain field and the gradient of the distortion field.

$$\begin{bmatrix} \varepsilon_{xx} & \varepsilon_{xy} \\ \varepsilon_{xy} & \varepsilon_{yy} \end{bmatrix} = \begin{bmatrix} \varepsilon'_{xx} & \varepsilon'_{xy} \\ \varepsilon'_{xy} & \varepsilon'_{yy} \end{bmatrix} \left\{ \begin{bmatrix} 1 & 0 \\ 0 & 1 \end{bmatrix} + \begin{bmatrix} p_{ux} & p_{uy} \\ p_{vx} & p_{vy} \end{bmatrix} \right\} \quad (6)$$

To assure symmetry of the final strain tensor, the shear strain is averaged as follow:

$$\varepsilon_{xy=}\varepsilon'_{xy} + \frac{1}{2}\left[\left(\varepsilon'_{xx}\, p_{uy} + \varepsilon'_{xy}\, p_{vy}\right) + \left(\varepsilon'_{xy}\, p_{ux} + \varepsilon'_{yy}\, p_{vx}\right)\right] \quad (7)$$

where $\varepsilon'_{ij}$ are the in-plane strains resolved by DIC software and previously corrected for magnification as proposed in "Quantifying Uncertainties in SEM Magnification" section, $p_{ux}$ and $p_{uy}$ are the derivatives of the horizontal distortion, and $p_{vx}$ and $p_{vy}$ are the derivatives of the vertical distortion, with respect to x and y. These gradients are computed at the same position and with the same subset size as used in the DIC software. For all the results presented in this paper, we have used Correlated Solutions Vic-2D (2009) for digital image correlation.

## Grid Accuracy and Resolution

In the example presented in the last section, we have plotted features equally spaced every 10 μm according to the grid readings, and now to check the grid spacing reliability, an additional experiment is described as follows. First, we took a series of five grid images as depicted in Fig. 12. The images were taken at different grid position. We moved the stage the following amount between images: (a)→(b) 20 μm left; (b)→(c) 20 μm down; (c)→(d) 20 μm down and 20 μm left; (d)→(e) 20 μm down and 20 μm left. The real stage displacement value is arbitrary, since any subset tile can be tracked in the code from the position with respect to the acquired image. The purpose of these experiments is to validate the certified equi-spaced grid targets, by comparing different regions across the grid and checking the reliability.

The disparity of the grid position was computed every 10 μm for each image, as sketched in Fig. 12 (e), following the procedure described in "Spatial Distortion Correction" section. In this case, we mapped 8 horizontal by 6 vertical points in each image starting at the same initial pixel positon. All images were acquired with the optimization procedures described before. In this case, we expect to have minimized drift distortion that is on the same level as the SEM noise. To analyze the accuracy of the grid targets, let's consider $S(x, y)$ to be the matrix formed by the pixel positions of the mapped points that are shown in the SEM image. If spatial distortion is a stationary inherent SEM distortion, as demonstrated in [8, 13], then it does not depend on the substrate, and it shall always present the same distortion. When translating the calibration grid, we will have new set of reference data on the substrate. By denoting $X_i(x, y)$, $i = 1, 2, 3, 4$ and 5, the position of the targets based on the grid pattern for each image $i$, the disparity matrix computed for each image will be given by:

$$D_i(x, y) = S(x, y) - X_i(x, y) \quad (8a)$$

If the hypothesis of fixed spatial distortion holds, then the calculated disparity $D_i(x, y)$ will be related with the true distortion $T_i(x, y)$ by:

$$T_i(x, y) = D_i(x, y) + G_i(x, y) \quad (8b)$$

where $G_i(x, y)$ is a matrix of Gaussian errors related with the SEM image noise. Therefore, due to the nature of Gaussian error, the true distortion can be estimated by:

$$\overline{T}_i(x, y) \approx \frac{\sum_{i=1}^{n} D_i(x, y)}{n} \quad (8c)$$

In the present case, $n = 5$. The error in the disparity measured by the independent set of images is given by:

$$G_i(x, y) = \overline{T}_i(x, y) - D_i(x, y) \quad (8d)$$

From the results of (equation (8d)), if the Gaussian errors are high, then either the grid does not possess the claimed accuracy or the noise and/or drift is not negligible as earlier stated. On the other hand, if the errors are on the order of the expected uncertainty, i.e. ~0.1%, then the grid targets are satisfactory accurate for the purpose of this work and the noise is sufficiently minimal.

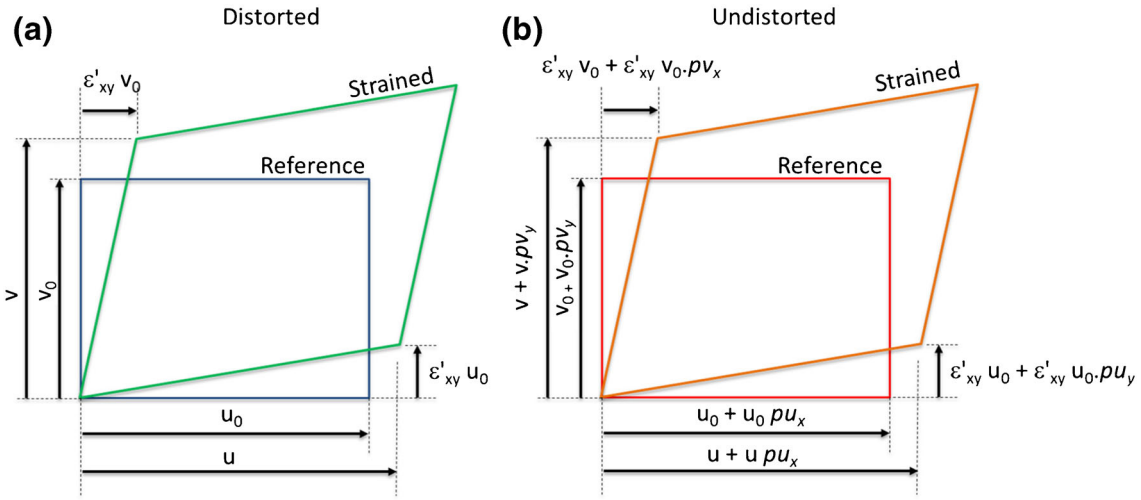


**Fig. 11** Represents (a) the original images and (b) a new system with distortion correction applied to both, reference and strained images

The Gaussian error based on (equation (8a-d)) was determined using the 5 images as exemplified in Fig. 12. The grid targets were obtained finding the center of a subset tile of 50 × 50 pixels every 10 μm. The targets are numbered from left to right and from top to bottom. The point on the top left is the reference target used to compute the distortion field.

Figure 13 shows the vertical and horizontal distortion Gaussian error plotted for all 48 mapped targets for the 5 independent images. From Fig. 13, we can see that the errors between disparity measurements are confined in a band from −0.1 to 0.1 pixel. The standard deviations for the Gaussian error of mapped points are 0.027 pixel for the horizontal distortions and 0.030 for vertical distortions. The maximum errors measured for horizontal and vertical distortions are 0.055 pixel and 0.1 pixel, respectively. Considering that the distance between targets (10 μm) is determined to be 325.143 pixels, the maximum percentage error between targets (determined by the ratio of 0.1 maximum pixel error by 325.143 pixel distance between targets) will be 0.03%. Therefore, we claim that the grid is sufficiently accurate to perform the spatial calibration as proposed, and the SEM noise is within the acceptable level, for target step of 10 μm at the tested resolutions.

Despite the Gaussian error being small, by looking at Fig. 13(b), we see a clear tendency of the noise to increase as the scan moves down (noted jumps from points 8 to 9, 16 to 17 and so on) for the vertical distortion within the same image.

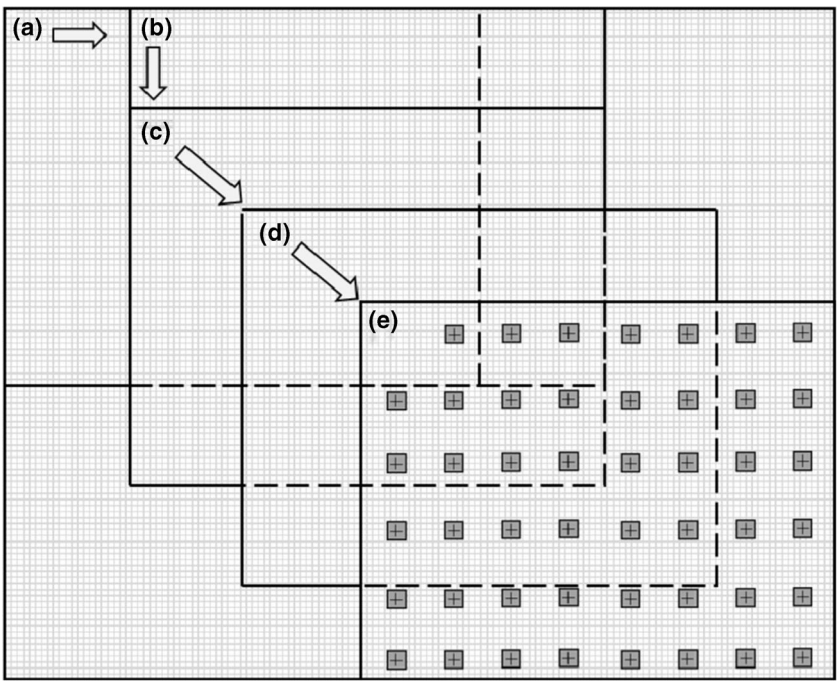


**Fig. 12** Sketch of cross check for grid accuracy. Five images were taken at different spots of a certified Pelcotec™ G-1C Silicon Calibration Specimen. Only the sketch of mapped points in image (e) is shown for simplicity

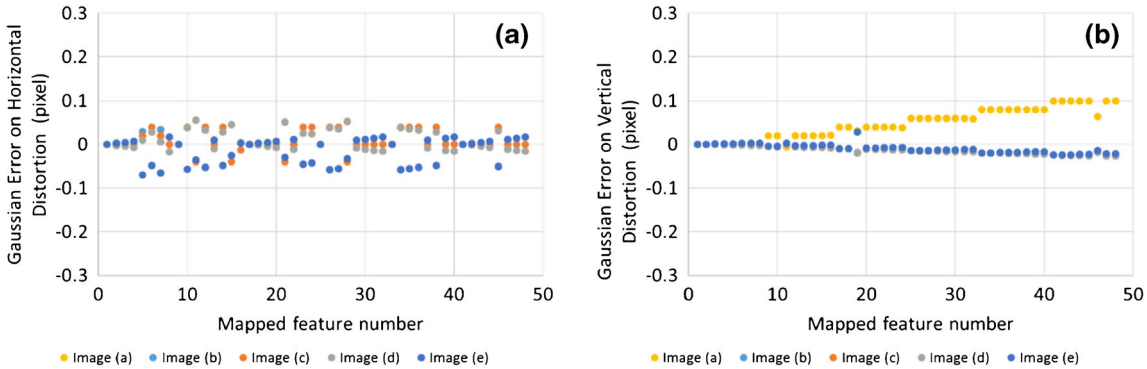


**Fig. 13** Gaussian error of defined image positions numbered 1 to 48 from left to right and from top to bottom as shown in Fig. 12, (a) horizontal and (b) vertical distortions

Interestingly, the first image shows a tendency of distortion in one direction, having the highest dispersion, and the other images show the opposite direction, but with values closer to the central average. For the horizontal distortion, the noise is random as seen in Fig. 13(a).

## Quantifying Uncertainties in SEM Magnification

As previously noted, when performing time consuming or interrupted tests, sequences of images are normally taken days or weeks apart. Every time the microscope is turned on, there might be a slight difference between the magnifications of the acquired images. The typical uncertainty defined by the SEM manufacturer for magnification, maintaining all parameters exactly the same, is on the order of 3%. The sources of this uncertainty are discussed by Watt [21]. For experimental mechanics of engineering alloys, this error can be far above the maximum localized strain being measured. One important technique to minimize this difference is to adopt the procedure of always starting from the highest magnification available in the SEM and then going to the desired magnification for the DIC characterization. Figure 14 depicts a typical hysteresis loop for magnification.

Figure 15 displays two grid images taken on a FEI NOVA nanoSEM on different days, with exactly the same acquisition parameters. This pair of images presented the largest difference in magnification during our experiments, and it was chosen to clearly exemplify a recurring issue. The distortion code presented in "Spatial Distortion Correction" section can be used to determine the correct calibration for each image. Figure 15(a) displays 90 μm in 1942 pixels, having an average of 46.3 nm per pixel, while Fig. 15(b) displays 90 μm in 1906 pixels, with an average of 47.2 nm per pixel. If the same difference in magnification is present in the DIC images, there will be an erroneous average linear strain of −1.85% in the final analysis.

During each DIC image acquisition session, the grid image must be acquired for magnification correction purpose. Since we are using the certified grid for local corrections, we use the same grid to address the magnification correction that can be automated by implementing the set of (equations (6 and 7)) in addition to (equation (9)) that is described below. Both the axial and transverse strains must be corrected for magnification differences between the reference and strained images. No correction is necessary for the shear strain, as the shear strain will be properly corrected by the image distortion as proposed in "Spatial Distortion Correction" section. The correction for $\epsilon_{xx}$ and $\epsilon_{yy}$ will be:

$$\epsilon'_{xx} = \frac{\left(\epsilon_{xx_{V2D}} - \overline{\varepsilon}\right)}{1 + \overline{\varepsilon}} \tag{9a}$$

$$\epsilon'_{yy} = \frac{\left(\epsilon_{yy_{V2D}} - \overline{\varepsilon}\right)}{1 + \overline{\varepsilon}} \tag{9b}$$

where $\epsilon_{xx_{V2D}}$ and $\epsilon_{yy_{V2D}}$ are the DIC axial and transverse strains from Vic-2D (the DIC correlation package used in this

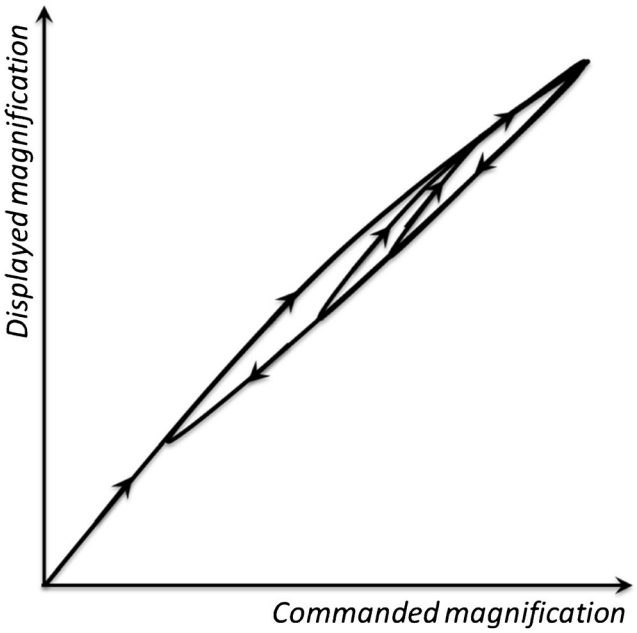


**Fig. 14** Typical hysteresis loops for the magnification in a SEM

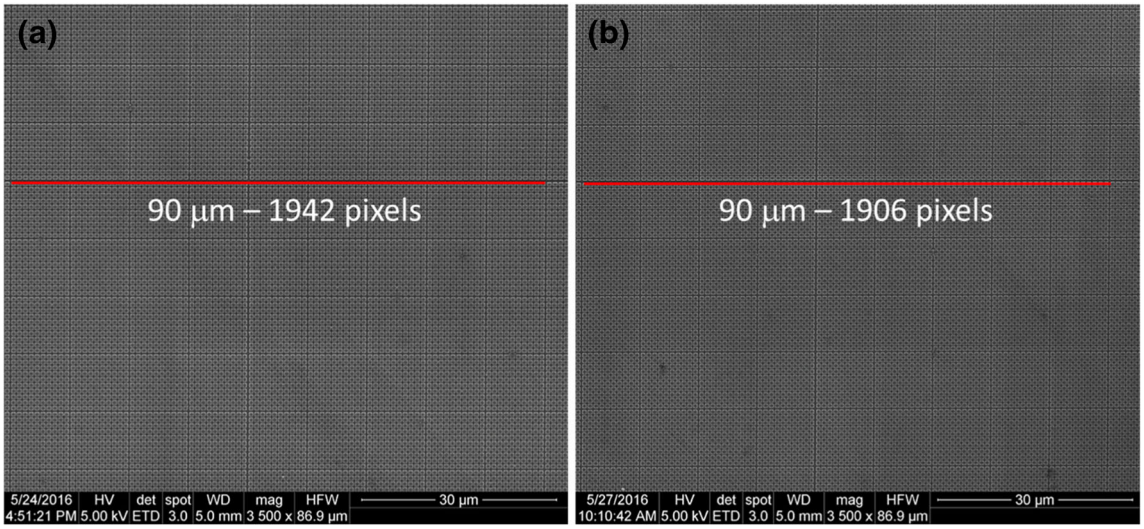


**Fig. 15** Grid images taken at different SEM sessions with exactly the same acquiring parameters

analysis) and $\bar{\varepsilon}$ is the erroneous magnification strain measured from the two grid images as explained before. In this case, the differences in magnification are consistent in both $x$ and $y$ directions.

If the axial engineering strains are measured with accuracy during the ex-situ DIC experiment, for instance by use of an extensometer, the final DIC average strains can be checked for similarity. If the average DIC strain is too far from the mechanical measured residual strain, then it is more likely a consequence of an unmatched magnification between the reference and strained images. The correction proposed in (equation (9)) shall bring the average strain back to the expected value. After this algebraic manipulation of the strain field, the local distorting correction proposed in "Spatial Distortion Correction" section must be applied.

## Results

Figure 16 illustrates the computed $\boldsymbol{u}$ and $\boldsymbol{v}$ displacement field obtained from the center portion of the calibration grid shown in Fig. 8. The consistent increase in $\boldsymbol{u}$-distortion in the y direction is due to the orthogonality issue during SEM acquisition, as discussed before. The magnitude of the $\boldsymbol{v}$-distortion is smaller than the $\boldsymbol{u}$-distortion, but exhibits more variation in the x and y directions.

A Matlab code was written to prescribe the distortion correction gradient seen in Fig. 16 onto the DIC results from Vic-2D, after proper magnification correction as proposed in "Quantifying Uncertainties in SEM Magnification" section. This code was first used in a calibration phase for resolution check between two reference images. The objective of this procedure is to establish the minimum subset size for a maximum of 0.1% standard deviation, which is considered, for the purposes of this study, as an acceptable signal-to-noise error. We claim that if distortion corrections are performed, two reference images correlated during the initial setup procedure will present less noise, thus allowing reduced subset size during the DIC analysis. In this analysis, the pair of images were taken within the same SEM session, so they are not subjected to the discrepancy in the magnification values. The distortion correction was applied to this calibration phase results, for a Ni-based superalloy speckled with Ti nanopowder. The standard deviation is reduced by 0.03% from the original result, thus enabling the use of a smaller subset and therefore improving the spatial resolution of the measured strains while avoiding excessive strain dipoles, as discussed by Efstathiou et al. [1].

The results comparing the localized strain for both corrected and non-corrected DIC results, after the specimen is loaded to 0.7% strain at 300 °C are shown in Fig. 17. The subset for the corrected strain field was set as 0.6 µm (21 pixels), Fig. 17(a), while for the non-corrected strain field was set as 1.5 µm (51 pixels), Fig. 17(b), granting the same accuracy for both measurements; albeit the smaller subset size allows higher spatial resolution, which implies much more detailed strain localization measurements. In both cases, the filter size was set to 15 with a step size of 1 pixel. Figure 17(c) shows the speckle pattern used for DIC. The profiles represented by the red lines in Fig. 17 were plotted for comparison, as depicted in Fig. 18. As observed in Fig. 18, the corrected results enabled a sub-micron spatial resolution map of strain. On the other hand, for the distorted images, the strain values would be averaged over a region of a few microns.

Finally, the spatial distortion and magnification correction are applied to two case studies. We performed two experiments with different substrate and speckling method. First, a fatigue test was conducted on a Ti-6Al-4V specimen, speckled with gold nanoparticles [22]. The specimen and grid were

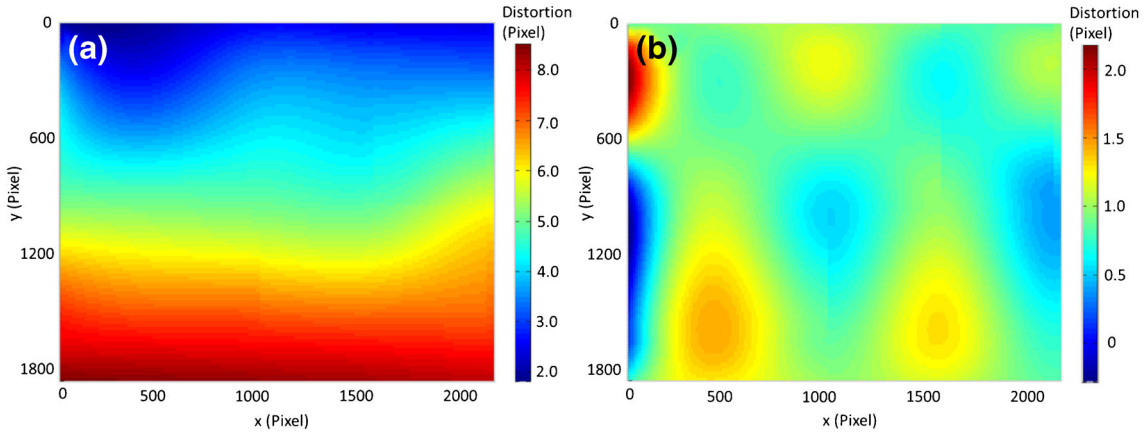


**Fig. 16** Distortion displacement field (a) ***u*** and (b) ***v*** from SEM image displayed in Fig. 8

imaged in the FEI Quanta 3D FEG field emission scanning electron microscope. The fatigue loading was monitored using a calibrated extensometer and the specimen was loaded to 1% strain followed by cyclic loading (in load control) at $R_\sigma = 0.05$, at room temperature. After 1000 cycles, the specimen was imaged within the SEM for ex-situ strain field determination.

The preliminary DIC results, due to erroneous magnification, showed an average strain of 1.43% for the area of interest with horizontal field widths of 60 μm, as shown in Fig. 19(a). Four images were taken at 8,000× and stitched together to form the entire field of view. The DIC average strain was above the expected value from the extensometer measurements. Based on the grid images taken along with the reference and strained images, the correction proposed in "Quantifying Uncertainties in SEM Magnification" section was applied, followed by the distortion correction ("Spatial Distortion Correction" section). The strain field, after correction is shown in Fig. 19(b). The average strain in this case was reduced to 0.88%, which is compatible with the mechanically measured values via the extensometer.

Second, a Ni-based superalloy was loaded to 0.7% strain and returned to zero load at 700 °C inside a vacuum chamber [23]. The specimen was speckled with 60 nm Titanium nanoparticles. After the test, the specimen was cooled to room temperature and imaged for DIC in the FEI Nova Nano Field Emission SEM. After magnification and distortion correction, the average strain in the mapped area was determined to be 0.37%, closer to the expected residual mechanical strain value. A comparison is shown in Fig. 19(c) prior to the spatial distortion and magnification correction and in Fig. 19(d) after applying these corrections.

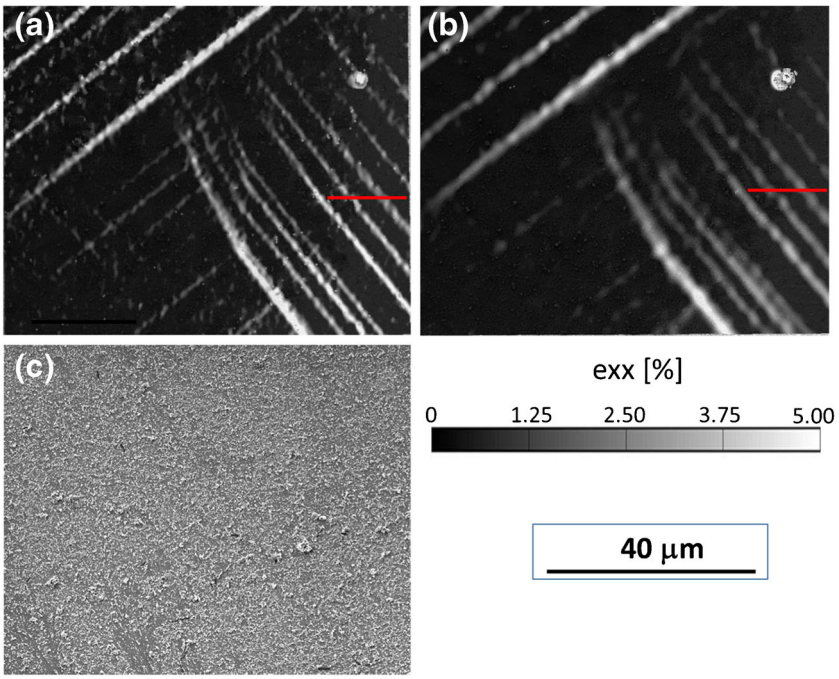


**Fig. 17** DIC of a Ni-based superalloy after permanent deformation at 300 °C: (a) spatial distortion correction and (b) non-correction; for both case the error was kept below 0.1% strain. (c) Ti nanopowder speckle pattern used for DIC

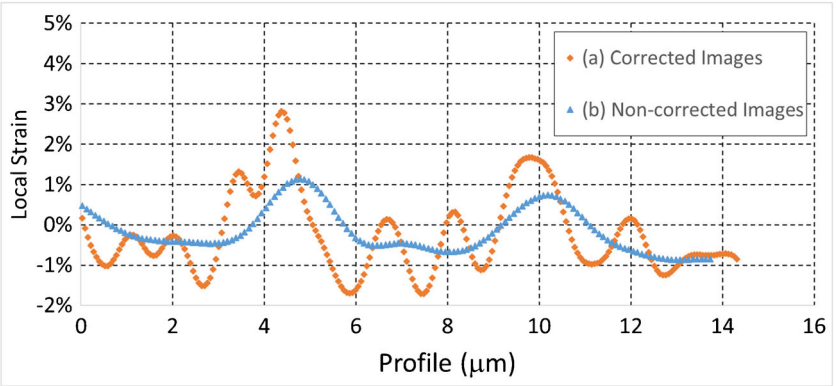


**Fig. 18** Strain profiles mapped over the red lines shown in Fig. 16

The two cases reported here serve as examples of the necessary distortion correction for SEM –DIC analysis, thus resulting in highly reliable strain maps with the ability to correlate strain using smaller sub-sets thereby providing higher resolution. In this procedure, a general framework is established that can be applied in any ex-situ SEM-DIC experiment, with the protocol established to focus on the nuances of ex-situ strain maps.

## Conclusion

High resolution DIC measurements obtained via SEM images enable sub-grain level resolution of strain and quantification of individual slip bands. However, researchers have shown that the resolution and accuracy of the measurements may be compromised by the inherent electromagnetic distortion of SEM images, giving rise to erroneous results. In this paper, we emphasize a systematic distortion correction protocol for long duration or ex-situ DIC measurements. We have discussed (i) the importance of minimizing noise during acquisition, since any perturbation caused by random effects cannot be predicted or corrected, (ii) properly grounding the specimen as a key step to minimize drift, and (iii) optimum parameters that allow increased signal-to-noise ratios according to the material and type of speckles in use.

A procedure to account for spatial distortions is introduced by using a certified grid and an image-based feature identification procedure to compute the distortion displacement field for the calibration image. The accuracy of the certified grid was tested and determined to be 0.03%, thus providing a reliable tool for correcting spatial distortions. Previous protocols are based on rigid body motion of the specimen to capture spatial distortions, which inherently relies on the precision of the SEM translational stage. The reliability of the calibration grid in the current study is better than that of traditional SEM translational stages. This displacement field is then applied to the DIC results thereby increasing the resolution of the

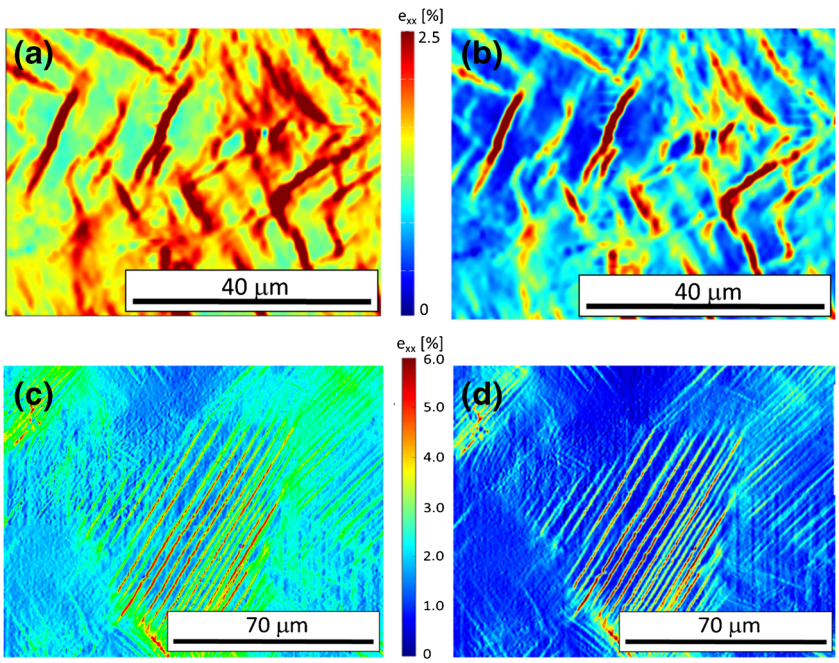


**Fig. 19** (a,b) Ti-6Al-4V specimen after 1000 fatigue cycles ($\sigma_{max}$ = 1050 MPa, $R_\sigma$ = 0.05): (a) without any correction and (b) after magnification and spatial distortion correction. (c,d) Ni-based superalloy specimen after 0.7% strain at 700 °C: (c) without any correction and (d) after magnification and spatial distortion correction. Fields of view on both specimens are composed of four images stitched together

computed strain fields (by utilization of a smaller subset size), while keeping the strain error below 0.1%. In other words, the uncertainty in the accuracy of the reference grid is approximately a third of the standard deviation of error during the image correlation analysis.

Another important aspect of this study, especially in application to ex-situ or long duration DIC experiments is the uncertainty quantification of the reported SEM magnification. According to the SEM manufacturer, the uncertainty for the reported magnification value, given all other parameters are kept constant, is on order of 3%. It is observed that two grid images acquired at the *same reported* magnification displayed a difference in strain of 1.85%, which is fictitious, and can dominate the underlying deformation strains in the sample that the DIC experiment is intended to quantify. This fake strain can be removed by taking reference images during each SEM sessions. These images are compared and the offset and amplification is properly applied to the DIC results. Finally, it is important to mention that SEM images are subjected to several internal and external variations due to variables, in which the user has little control over. Therefore the methodology reported in this manuscript provides a means to ensure consistency of the measured data. The reported procedure is intended to provide a systematic methodology, which can be applied to any SEM system and is suitable over a wide range of magnification values.

**Acknowledgements** Support for this work was provided by Rolls-Royce Corporation, DARPA (N66001-14-1-4041), the National Science Foundation (CMMI 13-34664), and the Office of Naval Research, (N00014-14-1-0544). The authors would like to thank: John Rotella from Purdue's ACME$^2$ group for his help on processing the images; Jan Eberle from Purdue for his help in better understanding the principles of SEM; and Professor Samantha Daly from the University of California at Santa Barbara for discussions on this topic. All electron microscopy was performed with the help of staff in the Life Science Microscopy Facility, Purdue University.

## Appendix

This paper provides a systematical protocol for distortion corrections (due to inherent electromagnetic spatial distortion or inaccurate displayed magnification values). The aforementioned procedures were developed for long duration, ex-situ experiments, in which the referenced and strained images are taken in separate SEM sessions and to minimize spatial distortion in SEM systems in which the *xyz* translational position stage has low resolution. To ensure this procedure is repeatable and easy to implement by future users, Table 1 provides a concise summary of the distortion correction protocol.

**Table 1** Summary guideline for the bias correction of SEM-DIC

| # | Step | Reason | Reference |
|---|---|---|---|
| 1 | Define the proper accelerating voltage. | Lower accelerating voltage provides better contrast on the surface speckles. Higher accelerating voltage will reduce external interference. | Ref. [10] |
| 2 | Define the lowest possible current (combination spot size, dwell time, and aperture) by keeping one parameter constant and systematically changing the other two parameters, and then repeating to toggle through the possible parameter combinations. | Minimize DIC subset size for a satisfactory standard deviation of strain between a pair of images. | "Drift Minimization and Appropriate Parameters for Noise Reduction" section |
| 3 | Place and ground specimen and adjacent, standard certified grid in the holder. | Minimize drift, determine the distortion field, and have an accurate reference for magnification. | "Drift Minimization and Appropriate Parameters for Noise Reduction" section |
| 4 | Take sample reference images with the proper field of view to resolve features of interest. | Digital image correlation reference. | |
| 5 | Take image of the grid with exactly the same parameters and working distance during the same session as Step 4. | Map the distortion field and have an accurate reference for run-time magnification calibration. | "Spatial Distortion Correction" section |
| 6 | Calculate the gradients of spatial distortion field from the certified grid image. | Gradients will be applied to the final DIC strain field. | "Spatial Distortion Correction" section and (equations (2-5)) |
| 7 | Repeat Steps 4 and 5 after the sample has been deformed. | Get sequence of images for DIC strain fields. | |
| 8 | Calculate and correct magnification as necessary for correlated images. | Slight differences in magnification can lead to large errors in the reported strain field. | "Quantifying Uncertainties in SEM Magnification" section and (equation (9)) |
| 9 | Apply the distortion correction to the strain field. | Spatial distortion can lead to erroneous localized strain measurements. | "Spatial Distortion Correction" section and (equations (6-7)) |

## References


1. Efstathiou C, Sehitoglu H, Lambros J (2010) Multiscale strain measurements of plastically deforming polycrystalline titanium: role of deformation heterogeneities. Int J Plast 26(2010):93–106. doi:10.1016/j.ijplas.2009.04.006
2. Abuzaid WZ, Sangid MD, Carroll JD, Sehitoglu H, Lambros J (2012) Slip transfer and plastic strain accumulation across grain boundaries in Hastelloy X. J Mech Phys Solids 60(6):1201–1220
3. Tschopp MA, Bartha BB, Porter WJ, Murray PT, Fairchild SB (2009) Microstructure-Dependent Local Strain Behavior in Polycrystals through In-Situ Scanning Electron Microscope Tensile Experiments. Metall Mater Trans A: Phys Metall Mater Sci 40(10):2363–2368. doi:10.1007/s11661-009-9938-6
4. Carter JLW, Zhou N, Sosa JM, Shade PA, Pilchak AL, Kuper WM, Wang Y, Fraser HL, Uchic MD, Mills MJ (2012) Characterization of strain accumulation at grain boundaries of nickel based superalloys. Superalloys 2012: 12th International Symposium on Superalloys (TMS), pp 43–52. doi:10.1002/9781118516430.ch5
5. Di Gioacchino F, Quinta da Fonseca J (2013) Plastic Strain Mapping with Sub-Micron Resolution Using Digital Image Correlation. Exp Mech 53(5):743–754. doi:10.1007/s11340-012-9685-2
6. Esquivel J, Sangid MD (2015) Digital Image Correlation of Heterogeneous Deformation in Polycrystalline Material with Electron Backscatter Diffraction. Microsc. Microanal. 21 (Suppl 3), 21 (0583): 1167–68. doi:10.1017/S1431927615006625
7. Kammers A, Daly S (2011) Experimental investigation of deformation mechanisms present in ultrafine-grained metals. In: Proulx T (ed) MEMS and nanotechnology, Volume 44. Conference Proceedings of the Society for Experimental Mechanics Series. Springer, New York, pp 105–10. doi:10.1007/978-1-4614-0210-7
8. Sutton MA, Li N, Garcia D, Cornille N, Orteu JJ, McNeill SR, Schreier HW, Li X, Reynolds AP (2007) Scanning Electron Microscopy for Quantitative Small and Large Deformation Measurements Part II: Experimental Validation for Magnifications from 200 to 10,000. Exp Mech 47(6):789–804. doi:10.1007/s11340-007-9041-0
9. Sutton MA, Li N, Joy DC, Reynolds AP, Li X (2007) Scanning Electron Microscopy for Quantitative Small and Large Deformation Measurements Part I: SEM Imaging at Magnifications from 200 to 10,000. Exp Mech 47(6):775–787. doi:10.1007/s11340-007-9042-z
10. Sutton MA, Li N, Garcia D, Cornille N, Orteu JJ, McNeill SR, Schreier HW, Li X (2006) Metrology in a Scanning Electron Microscope: Theoretical Developments and Experimental Validation. Meas Sci Technol 17(10):2613. doi:10.1088/0957-0233/17/10/012
11. Hitachi High-Technologies Corporation (2013) Ultra-high Resolution Scanning Electron Microscope SU8200 Series. Main specifications. www.hitachi-hitec.com/global/em/. Tokyo
12. Kammers AD, Daly S (2013) Self-Assembled Nanoparticle Surface Patterning for Improved Digital Image Correlation in a Scanning Electron Microscope. Experimental Mechanics, 1–15. doi:10.1007/s11340-013-9734-5.
13. Kammers AD, Daly S (2013) Digital image correlation under scanning electron microscopy: methodology and validation. Exp Mech 53.9:1743–1761
14. Stinville JC, Vanderesse N, Bridier F, Bocher P, Pollock TM (2015) High Resolution Mapping of Strain Localization near Twin Boundaries in a Nickel-Based Superalloy. Acta Mater 98:29–42. doi:10.1016/j.actamat.2015.07.016
15. Dai X, Xie H (2013) High-accuracy magnification calibration for a microscope based on an improved discrete Fourier transform. Opt Eng 52(11):1328–1342. doi:10.1117/1.OE.52.11.114102
16. Tortonese M, Guan Y, Prochazka J (2003) NIST-traceable calibration of CD-SEM magnification using a 100-nm pitch standard. Proc SPIE - Int Soc Opt Eng 5038:711–718. doi:10.1117/12.482648
17. Vladar AE (1999) Time-Lapse Scanning Electron Microscopy for Measurement of Contamination Rate and Stage Drift. Scanning 21: 191–196
18. Stinville JC, Echlin MP, Texier D, Bridier F, Bocher P, Pollock TM (2016) Sub-Grain Scale Digital Image Correlation by Electron Microscopy for Polycrystalline Materials during Elastic and Plastic Deformation. Exp Mech 56(2):197–216. doi:10.1007/s11340-015-0083-4
19. Marschallinger R, Topa D (1997) Assessment and Correction of Geometric Distortions in Low-Magnification Scanning Electron Microscopy Images. Scanning 19:36–41
20. Charbal A, Dufour J-E, Guery A, Hild F, Roux S, Vincent L, Poncelet M (2016) Integrated Digital Image Correlation considering gray level and blur variations: Application to distortion measurements of IR camera. Opt Lasers Eng 78:75–85. doi:10.1016/j.optlaseng.2015.09.011
21. Watt IM (1997) The Principles and Practice of Electron Microscopy. Chapter 5. 189-200. Second Edition. Cambridge University Press. ISBN 0 521 43591 9. New York
22. Book TA, Sangid MD (2016) Strain Localization in Ti-6Al-4V Widmanstätten Microstructures Produced by Additive Manufacturing. Mater Charact 122:104–112. doi:10.1016/j.matchar.2016.10.018
23. Mello AW, Nicolas A, Sangid MD (2017) Fatigue strain mapping via digital image correlation for Ni-based superalloys: the role of thermal activation on cube slip. Mater Sci Eng A 695:332–341. doi:10.1016/j.msea.2017.04.002